

# $\chi^2$ Analysis of Supersymmetric Models\*

Damien M. Pierce<sup>a</sup> and Jens Erler<sup>b</sup>

<sup>a</sup>Stanford Linear Accelerator Center, Stanford University, Stanford, California 94309, USA

<sup>b</sup>Institute for Particle Physics, University of California, Santa Cruz, California 95064, USA

We discuss the results of a global fit to precision data in supersymmetric models. We consider both gravity- and gauge-mediated models. As the superpartner spectrum becomes light, the global fit to the data typically results in larger values of  $\chi^2$ . We indicate the regions of parameter space which are excluded by the data. We discuss the additional effect of the  $B(B \rightarrow X_s \gamma)$  measurement. Our analysis excludes chargino masses below  $M_Z$  in the simplest gauge-mediated model with  $\mu > 0$ , with stronger constraints for larger values of  $\tan \beta$ .

## 1. Introduction

Low energy measurements can serve as useful probes of higher energy scales, because the virtual effects of heavy particles influence low energy observables. Hence, low energy measurements can constrain possible new physics scenarios. The most striking example of this effect was the “virtual top-quark discovery”. When the top-quark mass was first measured through direct production at the Tevatron, the precision electroweak data had already constrained the mass with about the same central value and uncertainty [1].

In the standard model some observables are sensitive to the square of the top-quark mass and the logarithm of the Higgs boson mass. Hence, both these masses can be constrained by precision data. In supersymmetric models, some observables are sensitive to the supersymmetric masses. Just as with  $m_t$  and  $M_H$ , there are values of supersymmetric parameters in conflict with measurements. We will discuss the results of a global fit to precision data in supersymmetric models.

Before discussing the supersymmetric case, we review the results of a global fit within the standard model. This serves as a useful barometer for comparison with the supersymmetric models. Also, the supersymmetric models reduce to the standard model as the supersymmetric mass scale

becomes large. The supersymmetric corrections decouple as  $M_Z^2/M_{\text{SUSY}}^2$  (or faster). The only remnant of supersymmetry in the large  $M_{\text{SUSY}}$  limit is the light Higgs boson mass (which remains a prediction of the model).

## 2. The observables

In the standard model we take as inputs the muon decay constant,  $G_\mu$ , the  $Z$ -boson mass,  $M_Z$ , the top quark mass,  $m_t$ , the Higgs boson mass,  $M_H$ , the electromagnetic coupling,  $\alpha$ , and the strong coupling,  $\alpha_s$ . The last two couplings are taken in the  $\overline{\text{MS}}$  scheme at the  $Z$ -scale.

Given these six inputs<sup>2</sup> we have predictions for all other observables in the standard model. We consider the list of observables below, and find the values of the five inputs<sup>3</sup> which minimize the total  $\chi^2$ . In this way we find the best fit values of the input parameters and the standard model predictions for all the observables.

The observables we include in our  $\chi^2$  are

- Line-shape and lepton asymmetries<sup>4</sup>. These are the  $Z$ -mass, the  $Z$ -width, the peak hadronic cross-section, the ratio of the hadronic width to the leptonic

\*Talk given by D.M.P. at the 5th International Conference on Supersymmetries in Physics (SUSY 97), Philadelphia, Pennsylvania, May 27-31, 1997. D.M.P. is supported by Department of Energy contract DE-AC03-76SF00515.

<sup>2</sup>We need to specify the remaining fermion masses as well, but the predictions for the observables we consider are not very sensitive to these inputs.

<sup>3</sup>Because of the small error, we take  $G_\mu$  as a fixed input.

<sup>4</sup>We include the correlations among these nine observables.

	Measurement	Standard Model	Pull
$M_Z$ [GeV]	$91.1863 \pm 0.0019$	91.1862	0.0
$\Gamma_Z$ [MeV]	$2494.7 \pm 2.6$	2496.9	-0.9
$\sigma_h$ [nb]	$41.489 \pm 0.055$	41.467	0.4
$R_e$	$20.756 \pm 0.029$	20.757	0.0
$R_\mu$	$20.795 \pm 0.029$	20.757	1.0
$R_\tau$	$20.831 \pm 0.029$	20.802	0.5
$A_{\text{FB}}^e$	$0.0161 \pm 0.0010$	0.0162	0.0
$A_{\text{FB}}^\mu$	$0.0165 \pm 0.0010$	0.0162	0.2
$A_{\text{FB}}^\tau$	$0.0204 \pm 0.0010$	0.0162	2.3
$\mathcal{A}_\tau(\tau)$	$0.1401 \pm 0.0067$	0.1469	-1.0
$\mathcal{A}_e(\tau)$	$0.1382 \pm 0.0076$	0.1469	-1.1
$\sin^2 \theta_{\text{eff}}^{\text{lept}}(\langle Q_{\text{FB}} \rangle)$	$0.2322 \pm 0.0010$	0.2315	0.7
$R_b$	$0.2177 \pm 0.0011$	0.2158	1.7
$R_c$	$0.1722 \pm 0.0053$	0.1723	0.0
$A_{\text{FB}}^b$	$0.0985 \pm 0.0022$	0.1030	-2.1
$A_{\text{FB}}^c$	$0.0735 \pm 0.0048$	0.0736	0.0
$\mathcal{A}_b$	$0.897 \pm 0.047$	0.935	-0.8
$\mathcal{A}_c$	$0.623 \pm 0.085$	0.667	-0.5
$A_{LR}$	$0.1548 \pm 0.0033$	0.1469	2.4
$\mathcal{A}_\mu$	$0.102 \pm 0.034$	0.147	-1.3
$\mathcal{A}_\tau$	$0.195 \pm 0.034$	0.147	1.4
$Q_W(\text{Cs})$	$-72.11 \pm 0.93$	-73.11	1.1
$Q_W(\text{TI})$	$-114.77 \pm 3.65$	-116.7	0.5
$M_W$ [GeV]	$80.402 \pm 0.076$	80.375	0.4
$m_t$ [GeV]	$175.6 \pm 5.0$	173.0	0.5
$\Delta\alpha_{\text{had}}$	$0.028037 \pm 0.000654$	0.02797	0.1

Table 1

Measured and best fit values of the observables in the standard model.

- widths, and the leptonic forward-backward asymmetries:  $M_Z$ ,  $\Gamma_Z$ ,  $\sigma_{\text{had}}$ ,  $R_{e,\mu,\tau}$ ,  $A_{e,\mu,\tau}^{FB}$ .
- $\tau$  polarization. The  $\tau$  decay analysis yields measurements of the  $\tau$  and  $e$  left-right asymmetries:  $\mathcal{A}_{\tau,e}(\tau)$ .
- Light quark charge asymmetry,  $\langle Q_{\text{FB}} \rangle$ , which yields a measurement of  $\sin^2 \theta_{\text{eff}}^{\text{lept}}$ .
- $b$  and  $c$  quark results. These are the ratios of the heavy quark widths to the total hadronic width, and the heavy quark forward-backward asymmetries (polarized at the SLC):  $R_{b,c}$ ,  $A_{b,c}^{FB}$ ,  $\mathcal{A}_{b,c}$ .
- Leptonic left-right asymmetries (total and forward-backward):  $A_{LR}$ ,  $\mathcal{A}_{\mu,\tau}$ .

- Atomic parity violation weak charges:  $Q_W(\text{Cs})$  and  $Q_W(\text{TI})$ .
- $W$ -boson mass, top-quark mass, and the light quark contribution to  $\alpha$ :  $M_W$ ,  $m_t$  and  $\Delta\alpha_{\text{had}}$ .

There are 26 observables included here. With 5 parameters in the fit, we are left with 21 degrees of freedom.

### 3. The standard model fit

In Table 1 we list the results of the standard model fit. We list the measured values with the errors<sup>5</sup> [2–7], the standard model predictions, and

<sup>5</sup>The data is current as of spring 1997.

the pull, which is defined to be the difference between the measured value and the standard model prediction, divided by the error. If we sum the squares of the pulls we obtain the  $\chi^2$  of the best fit, which in this case is 29.57. With 21 degrees of freedom, this corresponds to a probability of 10.1%. This means that if the standard model does describe the data, in a random variate (a set of measured values with central values distributed randomly in a Gaussian fashion) the probability that the  $\chi^2$  is greater than 29.57 is 10.1%. This 10.1% probability may sound low, but we consider it to be reasonable. Remember that the “best” we could hope for is 50% (higher than that would suggest that the data fits the predictions “too well”). In the days when  $R_b$  was  $3.5\sigma$  off, the goodness of the fit was much less than 1%.

The best fit values of some inputs are

$$m_t = 173 \pm 5 \text{ GeV} ,$$

$$\alpha_s = 0.122 \pm 0.003 ,$$

$$M_H = 93_{-57}^{+104} \text{ GeV} .$$

We show contours of constant  $\chi^2$  in the  $m_t - M_H$  plane in Fig. 1. The contours correspond to 68% and 90% confidence. We see that  $M_H$  is constrained to be less than 400 GeV at 95% CL.

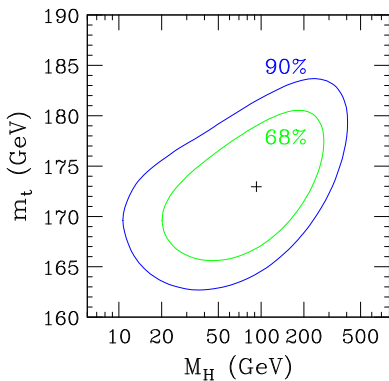


Figure 1. The standard model 68 and 90% CL contours in the  $m_t, M_H$  plane.

## 4. The supersymmetric analysis

There are two approaches to  $\chi^2$  analyses in supersymmetric models which one might consider. In the first approach one tries to repair the discrepancies seen between the data and the standard model [8]. For example, the standard model prediction for  $R_b$  used to be  $3.5\sigma$  off. One could find regions of supersymmetric parameter space where this discrepancy was repaired [9]. Now, however, there are no large ( $3\sigma$ ) discrepancies, and the largest deviations cannot be repaired by supersymmetry. This approach is no longer useful, since the supersymmetric corrections cannot reduce the  $\chi^2$  significantly, and one has to pay the price of the smaller number of degrees of freedom.

In the other approach, one notices that there are significant regions of parameter space where the supersymmetric corrections make the fit worse. Consider the plot<sup>6</sup> of  $\chi^2$  vs.  $M_{\text{SUSY}}$  in Fig. 2. At large  $M_{\text{SUSY}}$  the  $\chi^2$  approaches the standard model value (with the light Higgs mass determined as a function of the supersymmetric parameters). At smaller  $M_{\text{SUSY}}$ , the  $\chi^2$  typically rises; the unsuppressed supersymmetric radiative corrections can result in a terrible fit. Here we focus on this approach, elucidating the regions of parameter space where the  $\chi^2$  is so large that those points can be ruled out.

Notice there are two competing effects which will continue to determine the utility of this approach. As the data becomes more precise, the smaller errors will lead to larger values of  $\chi^2$  (assuming the discrepancies are real). At the same time, as more data is accumulated, the limits on the supersymmetric mass spectrum are increased. One must then consider larger values of the supersymmetric masses, and this leads to smaller values of  $\chi^2$ .

### 4.1. Three supersymmetric models

We will show the results of the  $\chi^2$  analysis in three supersymmetric models. The “minimal supergravity” model [10] is perhaps the most commonly considered high scale model. Here we take

<sup>6</sup>This plot corresponds to the “minimal supergravity” model with the universal soft parameters set to  $M_{\text{SUSY}}$ ,  $\tan\beta = 2$  and  $\mu > 0$ . Some region of the curve has superpartners lighter than the current limits.

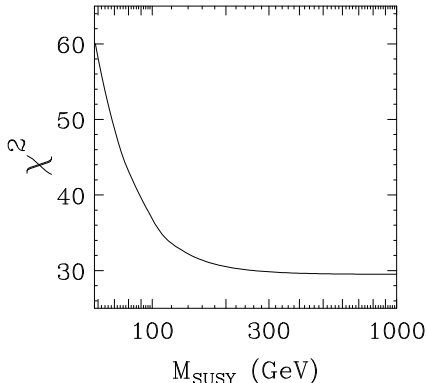


Figure 2.  $\chi^2$  vs.  $M_{\text{SUSY}}$ .

as boundary conditions at the GUT scale (the scale where  $g_1 = g_2$ ) a universal scalar mass  $M_0$ , a universal gaugino mass  $M_{1/2}$ , and a universal trilinear scalar coupling  $A_0$ . We also take as an input the ratio of vacuum expectation values of the two Higgs doublets,  $\tan\beta \equiv v_2/v_1$ , and the sign of the  $\mu$ -term.

Consider two assumptions which are necessary in order to arrive at the “minimal supergravity” model. First, one must assume a flat Kähler metric. Second, one assumes the universality of the scalar masses is maintained from the Planck scale to the GUT scale. Both of these assumptions seem artificial and unrealistic, especially the latter. However, they are useful for simplicity and economy, and in particular they guarantee that the model is free of potentially disastrous FCNC problems. Also, the running of the parameters between the Planck scale and the GUT scale is model dependent, so it makes sense that the minimal model assumes no running.

Models with gauge-mediated (GM) supersymmetry breaking [11] comprise a class which is automatically free of FCNC problems. Here, the supersymmetry breaking is communicated from the hidden sector to the visible sector through the interactions of the gauge fields and the messenger fields. In the minimal model the superpotential contains a singlet which acquires both a vev  $X$  and an  $F$ -term  $F_X$ . The singlet is coupled to the messenger fields, which are in a vector-like representation under the standard model gauge group.

The supersymmetric spectrum is proportional to  $\Lambda \equiv F_X/X$ , with dependence on the messenger field representation. We consider two models, a model with a  $5 + \bar{5}$  messenger sector and a model with a  $10 + \bar{10}$  messenger sector. The boundary conditions for the soft masses are applied at the messenger mass scale,  $M$ . Again, we take  $\tan\beta$  and the sign of  $\mu$  as inputs.

In both the supergravity and gauge-mediated models we impose radiative electroweak symmetry breaking [12]. Starting with a common positive Higgs boson mass-squared at the GUT scale or the messenger scale, we evolve the Higgs masses down to the weak-scale using the renormalization group equations (RGE’s) [13]. Because of the large top-quark Yukawa coupling, the mass-squared of the Higgs which couples to the top,  $m_{H_2}^2$ , is driven negative in the vicinity of the electroweak scale. This signals the breaking of electroweak symmetry, and requiring this to occur allows us to solve for the heavy Higgs boson mass and the Higgsino mass as a function of the input parameters:

$$m_A^2 = \frac{1}{\cos 2\beta} (m_{H_2}^2 - m_{H_1}^2) - M_Z^2 \quad (1)$$

$$\mu^2 = \frac{1}{2} \left[ \tan 2\beta (m_{H_2}^2 \tan \beta - m_{H_1}^2 \cot \beta) - M_Z^2 \right] \quad (2)$$

In the gauge-mediated models we implicitly assume that whatever mechanism is responsible for the generation of the  $B$  and  $\mu$  terms does not give rise to contributions to the soft scalar masses.

#### 4.2. The determination of $\chi^2$

The overview of the  $\chi^2$  analysis is as follows:

1. Pick starting values for  $(M_Z, m_t, \alpha, \alpha_s)$ .
2. Pick a random point in supersymmetric parameter space.
3. For fixed  $(M_Z, m_t, \alpha, \alpha_s)$  solve the supersymmetry model by iteration.

Here we have two-sided boundary conditions. We know the gauge and Yukawa couplings and  $\tan\beta$  at the weak scale and the

soft parameters at the high scale. We include full one-loop corrections in the evaluation of the gauge and Yukawa couplings, and in the Higgs sector (both the light Higgs boson mass and electroweak symmetry breaking).

4. Compute  $\chi^2$ . Here we include the full one-loop supersymmetric corrections to every observable, with two caveats:
  - We use the oblique approximation for the evaluation of atomic parity violation weak charges
  - The SUSY box diagrams are neglected in  $Z$ -pole observables
5. Minimize  $\chi^2$  with respect to  $(M_Z, m_t, \alpha, \alpha_s)$  for the fixed set of supersymmetric corrections.
6. If not converged, go to step 3.
7. Apply current limits on the superpartner and Higgs boson mass spectrum from direct searches. If this fails, disregard this point.

We include the current mass limits from CDF, D0 [14], and LEP II [15]. LEP II has produced new limits on the chargino mass, the slepton masses, the Higgs boson masses, and the light top-squark mass. Because the spectrum in high scale models is correlated, the CDF and D0 gluino and squark mass limits are typically irrelevant. For example, in the  $10 + \overline{10}$  gauge-mediated model, after imposing the limits on the chargino, Higgs bosons, and sleptons, we find that the squark and gluino masses are larger than 260 GeV. The direct search limits are 230 and 180 GeV, respectively [14].

### 4.3. The oblique approximation

We can give a concise description of the overall magnitude and relevance of the supersymmetric corrections by considering the oblique approximation. Most of the precision observables involve gauge boson exchange, and hence they receive universal (i.e. process and flavor-independent) corrections from the gauge boson self-energies.

With  $M_Z$ ,  $G_\mu$ , and  $\alpha$  as inputs, there are three independent linear combinations of gauge-boson self-energies which appear in physical observables in the lowest order of a derivative expansion. In some cases the full corrections are dominated by the oblique corrections. This might be expected, since the oblique corrections include contributions from every non-singlet superpartner, so they are enhanced by the number of generations and/or the number of colors. The non-oblique corrections (the fermion wave-function, vertex, and box corrections) arise from a limited set of diagrams, since the loops are constrained by the external fermion quantum numbers.

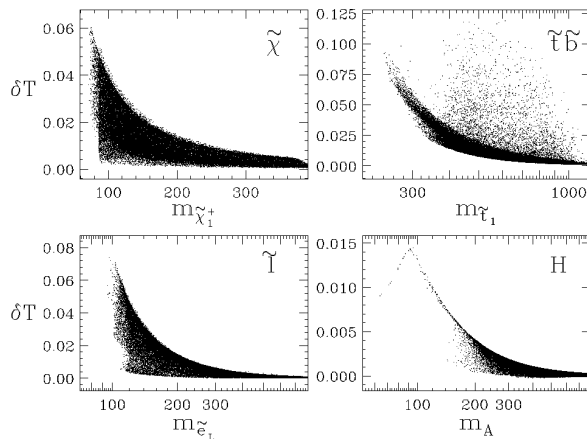


Figure 3. The contributions to  $T$  from the chargino/neutralino, stop/sbottom, slepton and Higgs sectors, in Figs. (a), (b), (c) and (d), respectively, vs. the representative masses. The masses are in units of GeV.

We parametrize the oblique corrections by  $S$ ,  $T$  and  $U$  [16]. These are given by the expressions [17]

$$S = \left[ \cos^2 \theta_W (F_{ZZ} - F_{\gamma\gamma}) \right. \quad (3)$$

$$\left. - \frac{\cos \theta_W}{\sin \theta_W} \cos 2\theta_W F_{\gamma Z} \right] \times \frac{4 \sin^2 \theta_W}{\alpha}$$

$$T = \left[ \frac{\Pi_{WW}(0)}{M_W^2} - \frac{\Pi_{ZZ}(0)}{M_Z^2} \right] \quad (4)$$

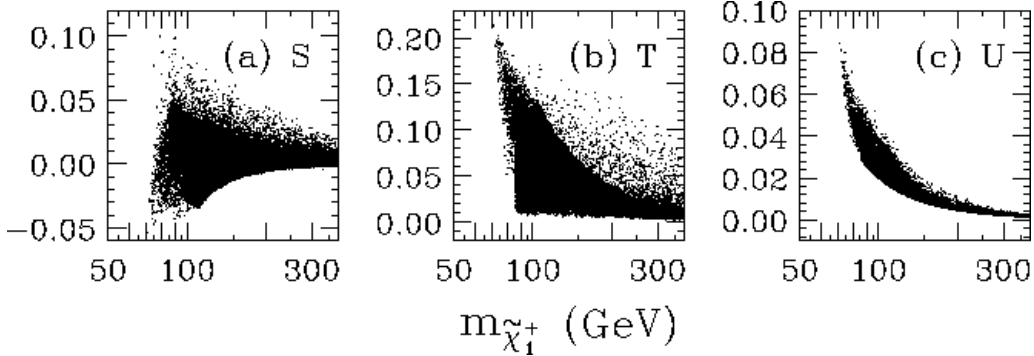


Figure 4. The supersymmetric contributions to  $S$ ,  $T$  and  $U$  in the supergravity model.

$$U = \left[ F_{WW} - \cos^2 \theta_W F_{ZZ} - \sin^2 \theta_W F_{\gamma\gamma} - \sin 2\theta_W F_{\gamma Z} \right] \times \frac{1}{\alpha} \quad (5)$$

where  $F_{ij} = (\Pi_{ij}(M_j^2) - \Pi_{ij}(0))/M_j^2$  (except  $F_{\gamma\gamma} = \Pi_{\gamma\gamma}(M_Z^2)/M_Z^2$ ).

The most important of these parameters is  $T$ . In Fig. 3 we show the contributions to  $T$  from the various supersymmetric sectors in the supergravity model. Each point in the scatter plots is a best fit at the randomly chosen point in supersymmetric parameter space, as described in Section 4.2. Fig. 3(a) shows the chargino/neutralino contribution vs. the light chargino mass, (b) shows the stop/sbottom contribution vs. the heavy stop mass, (c) shows the slepton contribution vs. the left-handed selectron mass, and (d) shows the supersymmetric Higgs boson contribution vs. the CP-odd Higgs boson mass. We note that all the sectors give positive contributions to  $T$  (also to  $U$ ). We see that the first three sectors contribute with the same order of magnitude (at most about 0.06, 0.12, and 0.07, respectively). The Higgs sector and the contributions of the first two generation squarks each contribute at most about 0.015.

If we add all these contributions together, we obtain the plots in Fig. 4. Here we show the total supersymmetric contributions to  $S$ ,  $T$  and  $U$  vs. the light chargino mass. The cancella-

tion between the slepton and chargino sectors results in typically smaller values for  $S$ . The SUSY contributions to  $S$ ,  $T$  and  $U$  are in the ranges  $(-0.05, 0.1)$ ,  $(0, 0.2)$ , and  $(0, 0.09)$ . For chargino masses above 300 GeV the decoupling results in suppressed contributions.

We illustrate the relevance of these corrections in Figs. 5. Here, in the  $T$ ,  $S$  plane, we show the 68% and 95% CL contours found by varying  $M_Z$ ,  $m_t$ ,  $\alpha$ ,  $\alpha_s$ , and  $U$ , with  $M_H$  fixed to its best fit value, in the standard model. On top of these contours we show scatter plots of the supersymmetric contributions to  $S$  and  $T$ . In Fig. 5(a) the minimal supergravity scatter plot is shown, in 5(b) the  $5 + \bar{5}$  gauge-mediated model scatter plot is shown, and the  $10 + \bar{10}$  GM model results are shown in 5(c). The point (0,0) is a part of each supersymmetric scatter plot, since this corresponds to the decoupled region of parameter space, where  $M_{\text{SUSY}}$  is large. As we decrease  $M_{\text{SUSY}}$ , the scatter moves up and to the right or left. One can get a feeling for the overall magnitude of the supersymmetric corrections here. The direct limits on the supersymmetric mass spectrum have significantly constrained the magnitude of the supersymmetric corrections. For example, in the  $5 + \bar{5}$  gauge-mediated model the contributions to  $S$  and  $T$  fall almost entirely inside the 68% contour.

#### 4.4. Full one-loop analysis

To rule out points in parameter space we need to consider the full one-loop supersymmetric corrections, not just the oblique corrections. The

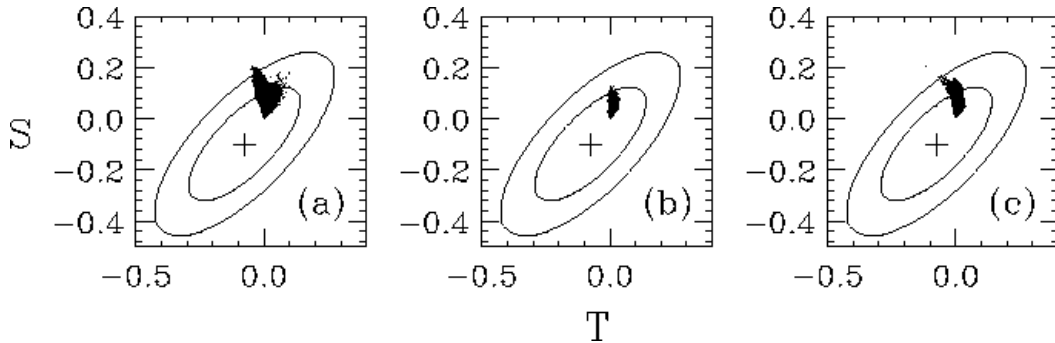


Figure 5. The supersymmetric contributions to  $S$  and  $T$  on the 68% and 95% standard model contours. The supergravity model, the  $5 + \bar{5}$  GM model, and the  $10 + \bar{10}$  GM model scatter plots are shown in Figs. (a), (b) and (c), respectively.

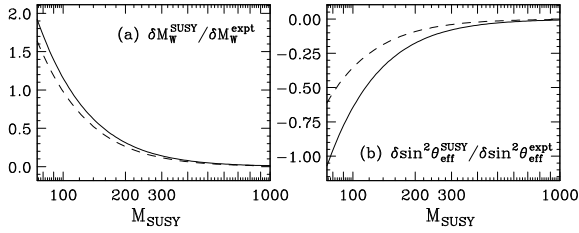


Figure 6. The supersymmetric corrections to (a)  $M_W$  and (b)  $\sin^2 \theta_{\text{eff}}^{\text{lept}}$  vs.  $M_{\text{SUSY}} = M_0 = M_{1/2} = A_0$ , with  $\tan \beta = 2$  and  $\mu > 0$ . The solid line shows the full one-loop correction, and the dashed line indicates the oblique approximation.

oblique approximation works well for some observables, but poorly for others. We illustrate this in Fig. 6. In Fig. 6(a) we show the  $W$ -boson mass vs.  $M_{\text{SUSY}}$  in the oblique approximation and the full one-loop result, and they are seen to be in good agreement (here we work in the supergravity model, define  $M_{\text{SUSY}} = M_0 = M_{1/2} = A_0$ , and set  $\tan \beta = 2$  and  $\mu > 0$ ). We show the correction in units of “pull” (that is, we divide the correction by the experimental error). In Fig. 6(b) we show the full and oblique  $\sin^2 \theta_{\text{eff}}^{\text{lept}}$ . Clearly the non-oblique corrections are significant in this case.

In the full one-loop supersymmetric analysis we have included an external constraint on the strong coupling,  $\alpha_s = 0.118 \pm 0.003$ , which we obtained by combining all except the  $Z$ -lineshape data [18].

The extent of the complete one-loop corrections

for each observable is shown in Fig. 7, where the horizontal lines indicate the range of values of each observable in the entire supersymmetric parameter space. The top line corresponds to the supergravity model, the middle line to the  $5 + \bar{5}$  GM model, and the bottom line to the  $10 + \bar{10}$  GM model. The small vertical line shows the value of the pull in the standard model.

Looking at this plot the general impression is that the supersymmetric corrections are unable to provide a significantly more satisfactory description of the data than the standard model. Some of the observables are seen to be irrelevant in the fit (i.e.  $R_c$ ,  $\mathcal{A}_c$ ,  $\mathcal{A}_b$ ,  $\mathcal{A}_\mu$ ,  $\mathcal{A}_\tau$ ,  $Q_W(\text{Cs})$  and  $Q_W(\text{Tl})$ ; the supersymmetric corrections to these observables are small relative to the experimental uncertainty). Of the observables with sizable corrections, some can reduce the SM discrepancies, ( $R_b$ ,  $A_{LR}$ ), while others can increase the SM discrepancies ( $\mathcal{A}_{e,\tau}(\tau)$ ,  $A_b^{FB}$ ). There are interesting correlations among the corrections to different observables. For example, the positive corrections to  $R_b$  (which reduce the SM discrepancy) are accompanied by positive corrections to  $A_b^{FB}$  (which lead to a larger discrepancy). We illustrate this in Fig. 8, which shows the  $A_b^{FB}$  pull vs. the  $R_b$  pull in the supergravity model.

The minimum  $\chi^2$  found in our random scan over parameter space is 29.6 for 19 degrees of freedom in the supergravity model. For both GM models, we find the minimum  $\chi^2$  values of 30.3 for 20 degrees of freedom. These correspond to

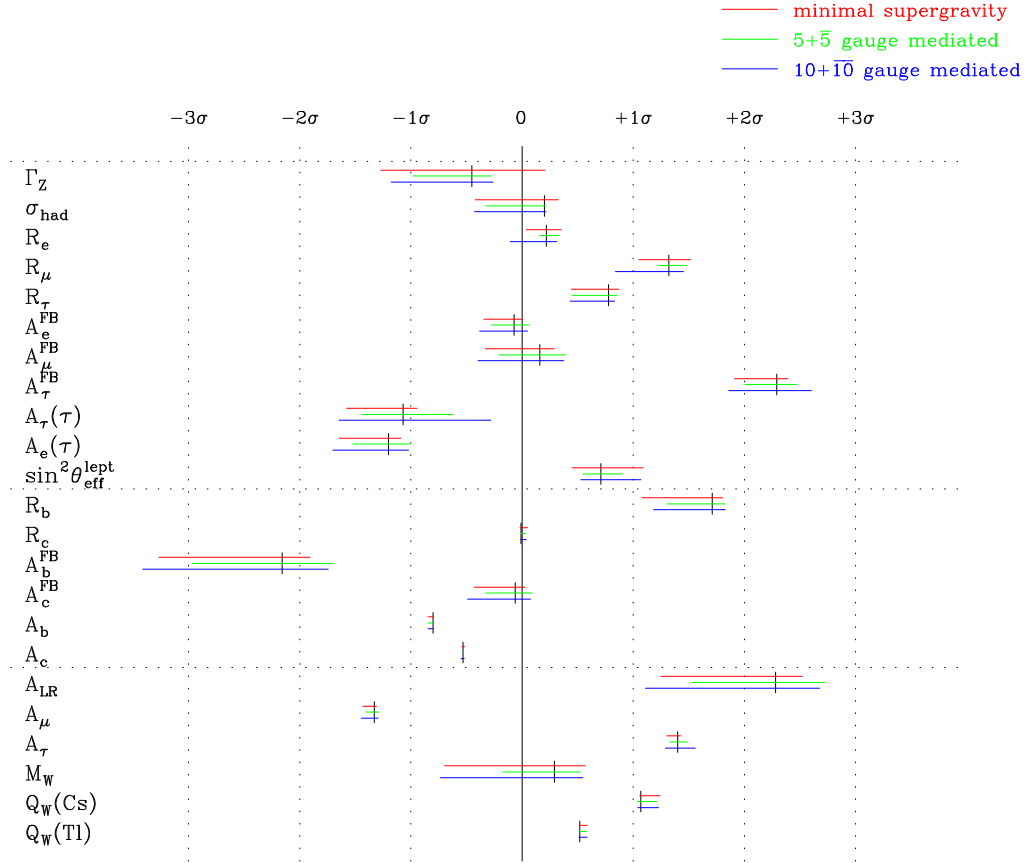


Figure 7. The maximal extent of the supersymmetric corrections to each observable, in units of pull. The horizontal lines correspond to, from top to bottom, the supergravity model, the  $5 + \bar{5}$  GM model, and the  $10 + \bar{10}$  GM model. The standard model pull is indicated by the small vertical lines.

goodness of fits of 5.8% and 6.5%, respectively. We can compare these numbers with the standard model goodness of fit of 10.9%. We see that the marginal reduction in  $\chi^2$  is more than compensated for by the increase in the number of input parameters.

What we are really interested in is the set of points with large values of  $\chi^2$ . Not counting the supersymmetry parameters as fit parameters, we deem a point in supersymmetric parameter space excluded if the goodness of the fit is less than 5%. In Fig. 9 we show the plots of  $\chi^2$  vs. the input parameters in the supergravity model, with  $\mu > 0$ . All points above the upper horizontal line are excluded at the 95% confidence level. Fig. 10 shows the same plot with  $\mu < 0$ . With  $\mu > 0$  there is significantly more parameter space ruled

out. We see that in the  $\mu > 0$  ( $\mu < 0$ ) case, there are no points excluded if  $M_{1/2} > 155$  (160) GeV, or  $M_0 > 160$  (100) GeV, or  $\tan \beta < 2.2$  (3). The excluded parameter space forms a complicated hyper-region.

We plot the full one-loop  $\chi^2$  vs.  $\Lambda$  in the  $5 + \bar{5}$  and  $10 + \bar{10}$  GM models in Fig. 11, with  $\mu > 0$ . We see that in the  $5 + \bar{5}$  model values of  $\Lambda < 30$  TeV are excluded. In the  $10 + \bar{10}$  case,  $\Lambda < 12$  TeV is excluded. In the  $5 + \bar{5}$  GM model with  $\mu < 0$  there are no points excluded by this analysis.

## 5. The $B \rightarrow X_s \gamma$ constraint

We now specially consider a very important observable. The CLEO measurement [19] of the rare decay  $B \rightarrow X_s \gamma$  yields the 90% confidence inter-



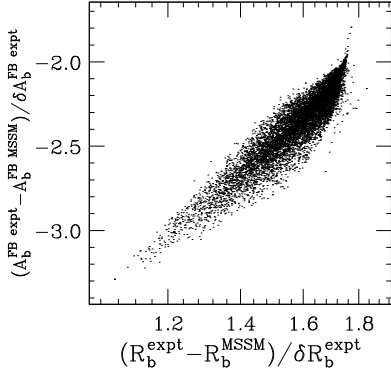


Figure 8. The pull of  $A_b^{FB}$  vs. the pull of  $R_b$  in the supergravity model.

val  $1.0 \times 10^{-4} < B(B \rightarrow X_s \gamma) < 4.2 \times 10^{-4}$ . This measurement imposes a significant constraint on supersymmetric models [20]. The charged Higgs loops and chargino loops give the largest contributions. The chargino contribution contains a term proportional to  $\mu \tan \beta$ , and it can be much larger than the standard model amplitude, and can be of either sign. Hence, the  $B \rightarrow X_s \gamma$  rate in supersymmetric models can be much larger or much smaller than the standard model prediction. This leads to very large values of  $\chi^2$  in some regions of parameter space (e.g.  $\mu > 0$  and large  $\tan \beta$ ). This is illustrated in Fig. 12, where we show the  $\chi^2$  before and after considering the  $b \rightarrow s \gamma$  constraint, in the  $5 + \bar{5}$  GM model, with  $\mu > 0$ . We see from Fig. 12(b) that we can exclude chargino masses below  $M_Z$  with the  $b \rightarrow s \gamma$  constraint. For larger values of  $\tan \beta$ , this constraint becomes stronger. We show in Fig. 13 the lower bounds on the lightest neutralino and lightest chargino masses vs.  $\tan \beta$ . There are corresponding bounds on the other superpartner masses. There are no such bounds in the case  $\mu < 0$ .

In the supergravity model the  $b \rightarrow s \gamma$  constraint does not yield such strong limits, because the parameter space has more freedom. Nevertheless, the additional region of parameter space which is excluded after including the  $b \rightarrow s \gamma$  measurement is significant. In particular, the  $\mu > 0$ , large  $\tan \beta$  region is severely constrained.

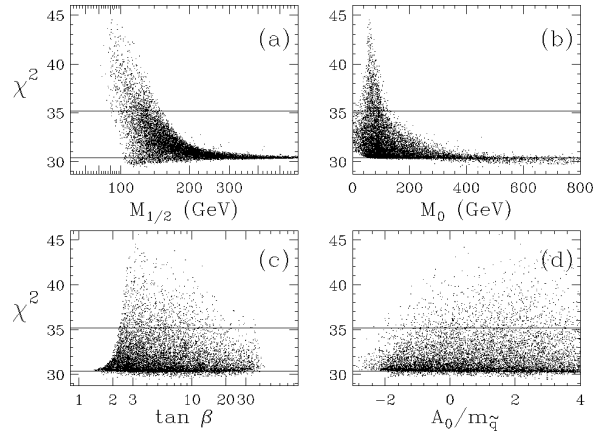


Figure 9. The total  $\chi^2$  vs. the input parameters in the supergravity model with  $\mu > 0$ . The lower horizontal line shows the minimum  $\chi^2$  in the standard model, with the external constraint,  $\alpha_s = 0.118 \pm 0.003$ , included. The points above the upper horizontal line are ruled out at the 95% CL.

## 6. Conclusions

Global fits to the world's precision data provide significant constraints on supersymmetric models. We gave an encapsulated view of the supersymmetric corrections by examining the oblique set. We then indicated the amount of parameter space which is excluded based on a full one-loop analysis. We found it important to include as many observables as possible in the fit, since different models, or different regions of parameter space in a given model, are more or less sensitive to different observables.

We showed the added sensitivity after including the  $b \rightarrow s \gamma$  measurement in the list of observables. The large  $\tan \beta$ ,  $\mu > 0$  region of parameter space was shown to be severely constrained.

Because the supersymmetric corrections decouple and the standard model with a light Higgs boson is consistent with the data, most of the supersymmetric parameter space is consistent with the data. Some regions of parameter space with light superpartners are excluded, but, on the other hand, there are points in parameter space

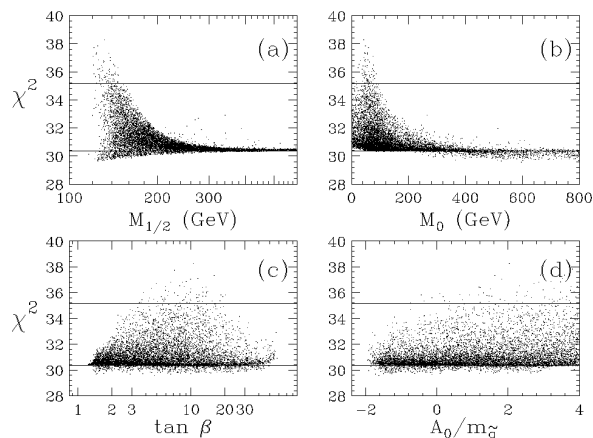


Figure 10. The same as Fig. 9, with  $\mu < 0$ .

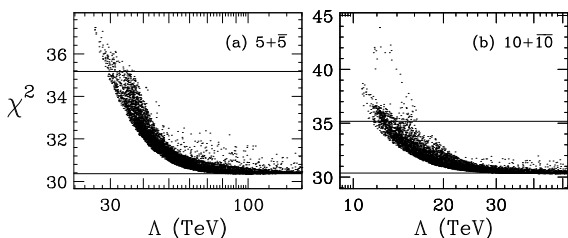


Figure 11. The total  $\chi^2$  vs.  $\Lambda$  in the (a)  $5 + \bar{5}$  and (b)  $10 + \bar{10}$  gauge-mediated models. The horizontal lines are as in Fig. 9.

with very light particles which are consistent with the data. In fact, the point in the supergravity model parameter space with the smallest  $\chi^2$  in our scan includes a light right-handed top-squark (55 GeV). So who knows what the next experiments will find?

### Acknowledgements

D.M.P. thanks the CERN theory group and the CERN computing center staff for generous hospitality.

### REFERENCES

1. J. Erler, P. Langacker, Phys. Rev. D52 (1995) 441.

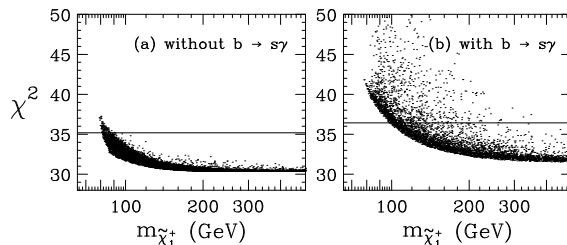


Figure 12. The total  $\chi^2$  vs. the light chargino mass in the  $5 + \bar{5}$  gauge-mediated model, with and without including the  $B(B \rightarrow X_s \gamma)$  constraint. The 95% CL region lies below the horizontal line.

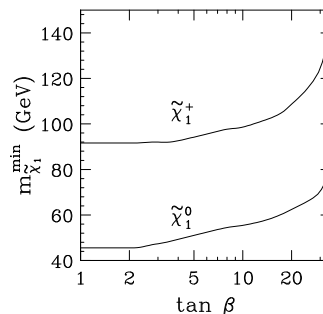


Figure 13. The lower bound on the lightest neutralino mass and the lightest chargino mass vs.  $\tan\beta$ , in the gauge-mediated model with the  $B(B \rightarrow X_s \gamma)$  constraint and  $\mu > 0$ .

2. A. Böhm for the ALEPH, DELPHI, L3 and OPAL Collaborations, talk presented at *32nd Rencontres de Moriond: Electroweak Interactions and Unified Theories*, Les Arcs, France, March 1997.
3. SLD Collaboration: K. Abe *et al.*, Phys. Rev. Lett. 78 (1997) 17, 78 (1997) 2075 and 79 (1997) 804; P.C. Rowson, talk presented at *32nd Rencontres de Moriond: Electroweak Interactions and Unified Theories*, Les Arcs, France, March 1997.
4. C. S. Wood *et al.*, Science 275 (1997) 1759; N. H. Edwards, S. J. Phipp, P. E. G. Baird, S. Nakayama, Phys. Rev. Lett. 74 (1995) 2654; P. A. Vetter, D. M. Meekhof, P. K. Majumder, S. K. Lamoreaux, E. N. Fortson, Phys. Rev. Lett. 74 (1995) 2658.
5. R. Raja for the D0 and CDF Collabora-

- tions, preprint FERMILAB-CONF-97-194-E, hep-ex/9706011; D0 Collaboration: B. Abbott *et al.*, preprint FERMILAB-PUB-97-172-E, hep-ex/9706014.
6. CDF Collaboration: F. Abe *et al.*, Phys. Rev. Lett. 65 (1990) 2243; *ibid.* 75 (1995) 11; Phys. Rev. D43 (1991) 2070; *ibid.* D52 (1995) 4784; D0 Collaboration: S. Abachi *et al.*, Phys. Rev. Lett. 77 (1996) 3309, and preprint FERMILAB-CONF-97-222-E, hep-ex/9706028.
  7. S. Eidelman, F. Jegerlehner, Z. Phys. C67 (1995) 585.
  8. G.L. Kane, Robin G. Stuart, James D. Wells, Phys. Lett. B354 (1995) 350; P.H. Chankowski, S. Pokorski, Phys. Lett. B366 (1996) 188; W. de Boer, A. Dabelstein, W. Hollik, W. Mösle, U. Schwickerath, hep-ph/9609209 and Z. Phys. C75 (1997) 627.
  9. M. Boulware, D. Finnell, Phys. Rev. D44 (1991) 2054; J.D. Wells, C. Kolda, G.L. Kane, Phys. Lett. B338 (1994) 219; X. Wang, J.L. Lopez, D.V. Nanopoulos, Phys. Rev. D52 (1995) 4116; D. Garcia, J. Sola, Phys. Lett. B354 (1995) 335; P.H. Chankowski, S. Pokorski, Nucl. Phys. B475 (1996) 3; J. Ellis, J.L. Lopez, D.V. Nanopoulos, Phys. Lett. B397 (1997) 88 and B372 (1996) 95.
  10. A. Chamseddine, R. Arnowitt, P. Nath, Phys. Rev. Lett. 49 (1982) 970; R. Barbieri, S. Ferrara, C. Savoy, Phys. Lett. B119 (1982) 343; L.J. Hall, J. Lykken, S. Weinberg, Phys. Rev. D27 (1983) 2359.
  11. M. Dine, W. Fischler, M. Srednicki, Nucl. Phys. B189 (1981) 575; S. Dimopoulos, S. Raby, Nucl. Phys. B192 (1981) 353; C. Nappi, B. Ovrut, Phys. Lett. B113 (1982) 175; L. Alvarez-Guamé, M. Claudson, M. Wise, Nucl. Phys. B207 (1982) 96.
  12. K. Inoue, A. Kakuto, H. Kamatsu, S. Takeshita, Prog. Theo. Phys. 68 (1982) 927; L. Alvarez-Gaumé, J. Polchinski and M.B. Wise, Nucl. Phys. B221 (1983) 495; J. Ellis, J.S. Hagelin, D.V. Nanopoulos, K. Tamvakis, Phys. Lett. B125 (1983) 275; L.E. Ibañez, C. Lopez, Nucl. Phys. B233 (1984) 511; L.E. Ibañez, C. Lopez, C. Muñoz, Nucl. Phys. B250 (1985) 218.
  13. M.E. Machacek, M.T. Vaughn, Nucl. Phys. B222 (1983) 83; *ibid.* B236 (1984) 221; *ibid.* B249 (1985) 70; I. Jack, Phys. Lett. B147 (1984) 405; Y. Yamada, Phys. Rev. D50 (1994) 3537; I. Jack, D.R.T. Jones, Phys. Lett. B333 (1994) 372; S. Martin and M. Vaughn, Phys. Lett. B318 (1993) 331; *ibid.*, Phys. Rev. D50 (1994) 2282.
  14. R. Culbertson, proceedings of the 5th International Conference on Supersymmetries in Physics (SUSY 97), Philadelphia, Pennsylvania, May 27-31, 1997.
  15. F. Cerutti, proceedings of the 5th International Conference on Supersymmetries in Physics (SUSY 97), Philadelphia, Pennsylvania, May 27-31, 1997.
  16. M.E. Peskin, T. Takeuchi, Phys. Rev. Lett. 65 (1990) 964; *ibid.* Phys. Rev. D46 (1992) 381.
  17. P.H. Chankowski, A. Dabelstein, W. Hollik, W.M. Mösle, S. Pokorski, J. Rosiek, Nucl. Phys. B417 (1994) 101.
  18. For a review see P. N. Burrows, Acta Phys. Polon. B28 (1997) 701.
  19. CLEO Collaboration: M.S. Alam *et al.*, Phys. Rev. Lett. 74 (1995) 2885.
  20. S. Bertolini, F. Borzumati, A. Masiero, G. Ridolfi, Nucl. Phys. B353 (1991) 591; F. Borzumati, Z. Phys. C63 (1994) 291; V. Barger, M.S. Berger, P. Ohmann, R.J.N. Phillips, Phys. Rev. D51 (1995) 2438; F. Gabbiani, E. Gabrielli, A. Masiero, L. Silvestrini, Nucl. Phys. B477 (1996) 321; D. Choudhury, F. Eberlein, A. Konig, J. Louis, S. Pokorski, Phys. Lett. B342 (1995) 180; J. Lopez, D. Nanopoulos, X. Wang, A. Zichichi, Phys. Rev. D51 (1995) 147; A. Ali, G.F. Giudice, T. Mannel, Z. Phys. C 67 (1995) 417; J.L. Hewett, J.D. Wells, Phys. Rev. D55 (1997) 5549; N.G. Deshpande, B. Dutta, S. Oh, Phys. Rev. D56 (1997) 519; H. Baer, M. Brhlik, Phys. Rev. D55 (1997) 3201.